NRIAG JOURNAL OF ASTRONOMY AND GEOPHYSICS
2022, VOL. 11, NO. 1, 282–292
https://doi.org/10.1080/20909977.2022.2085992



# Delineation of subsurface structures using gravity interpretation around Nabaa Al Hammara area, Wadi El Natrun, Egypt

Mahmoud S. Awad[a], Hassan H. El Kadi[b], Abbas M. Abbas and Sultan Awad Sultan Araffa[c]

[a]Department of Geoelectric and Geomagnetic, GEOLOG Surface Logging DMCC, Cairo, Egypt; [b]Geologic Department, Faculty of Sciences, Al Azhar University, Cairo, Egypt; [c]National Research Institute of Astronomy and Geophysics (NRIAG), Helwan, Cairo, Egypt

**ABSTRACT**

Nabaa El Hammra lies in the northeastern part of Wadi El-Natrun, characterised by low lands and most parts of this area are cultivated with different crops. In the current study, gravity data are used to investigate the subsurface structural features that can directly affect the configuration and distribution of groundwater aquifers and oil reservoirs accumulations. The present study aims to delineate the subsurface structural elements and to define the basins and basement uplifts, which can directly affect the flow of groundwater or oil accumulations. Gravity data are processed and filtered in diverse approaches to outlining the prevailed structure. The results of gravity data interpretation reveal that the studied area is affected by many structural features as NE-SW, NW-SE, N-S and E-W trends. These structural features caused barriers to the groundwater movement from or to the study area. The study revealed that the depth of the crystalline (Pre-Cambrian) rocks ranges from 3800 metres in the south part to 5300 metres in the northeastern region. Meanwhile, the basement rocks represent a bridge of shallow depth of northwest-southeast trend at the centre of the investigated area.

**ARTICLE HISTORY**
Received 18 March 2022
Revised 29 April 2022
Accepted 31 May 2022

**KEYWORDS**
Groundwater; gravity; structures trends; basement rocks; 3-D modelling

## 1. Introduction

The investigated area lies at the northeastern part of the Western Desert to the northeast of Wadi El-Natrun area between latitudes 30° 15` and 30° 38` North and longitudes 30° 08` and 30° 32` East. It is a part of Beheira governorate, about a few kilometres away from the west of Cairo-Alexandria desert road. The area extends for an average of 47 km × 42 km, and its approximate area is 1974 km$^2$ (Figure 1). The Wadi El Natrun area includes inland saline lakes, which extract some essential salts. These inland saline lakes contain different minerals, valuable minerals, and salts. The ancient Egyptians used different minerals such as carbonated sodium, which was extracted from Wadi El-Natrun; these Sodium Carbonates were required for the mummification process. Also, the Romans extracted silica for glass from Wadi El Natrun.

Moreover, Wadi El Natrun occupies significant areas used for agriculture purposes for different types of crops, which irrigate with groundwater at shallow depths. The study area has attracted many researchers to inspect its characteristics. Araffa et al. 2021a; Araffa et al, 2021b studied the hydrogeophysical behaviour of El Moghra area west of the current study area. Ibraheem Ismael et al. (2018) used aeromagnetic data to delineate the subsurface structures and estimate the depth of basement rocks ranging from 2.25 km to 5.43 km. On the other hand, some authors have applied the gravity method for variant prospects such as groundwater exploration, delineating structural elements, etc. (Abdel Zaher et al. 2018; Araffa et al. 2018; Elbarbary et al. 2021). The study area lies in Natrun basin, northeastern of Abu-Gharadig basin, east of Alamein basin, and north of El-Gendi basin; these areas contain many oil fields. For these reasons, the study area may be highly potential for oil accumulation.

## 2. Geologic- setting

The area under study is characterised by slightly undulating topography and higher land than the cultivated parts. The topographic map (Figure 1(b)) is constructed from the data of a digital elevation model. This map reveals differences in topographic features ranging between −21 and 115 m. The geomorphology of the study area is studied by many authors (Said 1962; Shata and El Fayoumi 1967; Abu E-IMS. 1971).

The geologic setting of the area under study is constructed from CONOCO (1987) (Figure 1(c)). The studied area is mainly dominated by sediments belonging to Cenozoic rocks. The Pliocene and Miocene sediments that represent the Tertiary rocks consist of clastic sediments such as sand and sandstone with clay intercalations. These Cenozoic rocks

**CONTACT** Sultan Awad Sultan Araffa sultan_awad@yahoo.com National Research Institute of Astronomy and Geophysics (NRIAG), 11722, Helwan, Cairo, Egypt

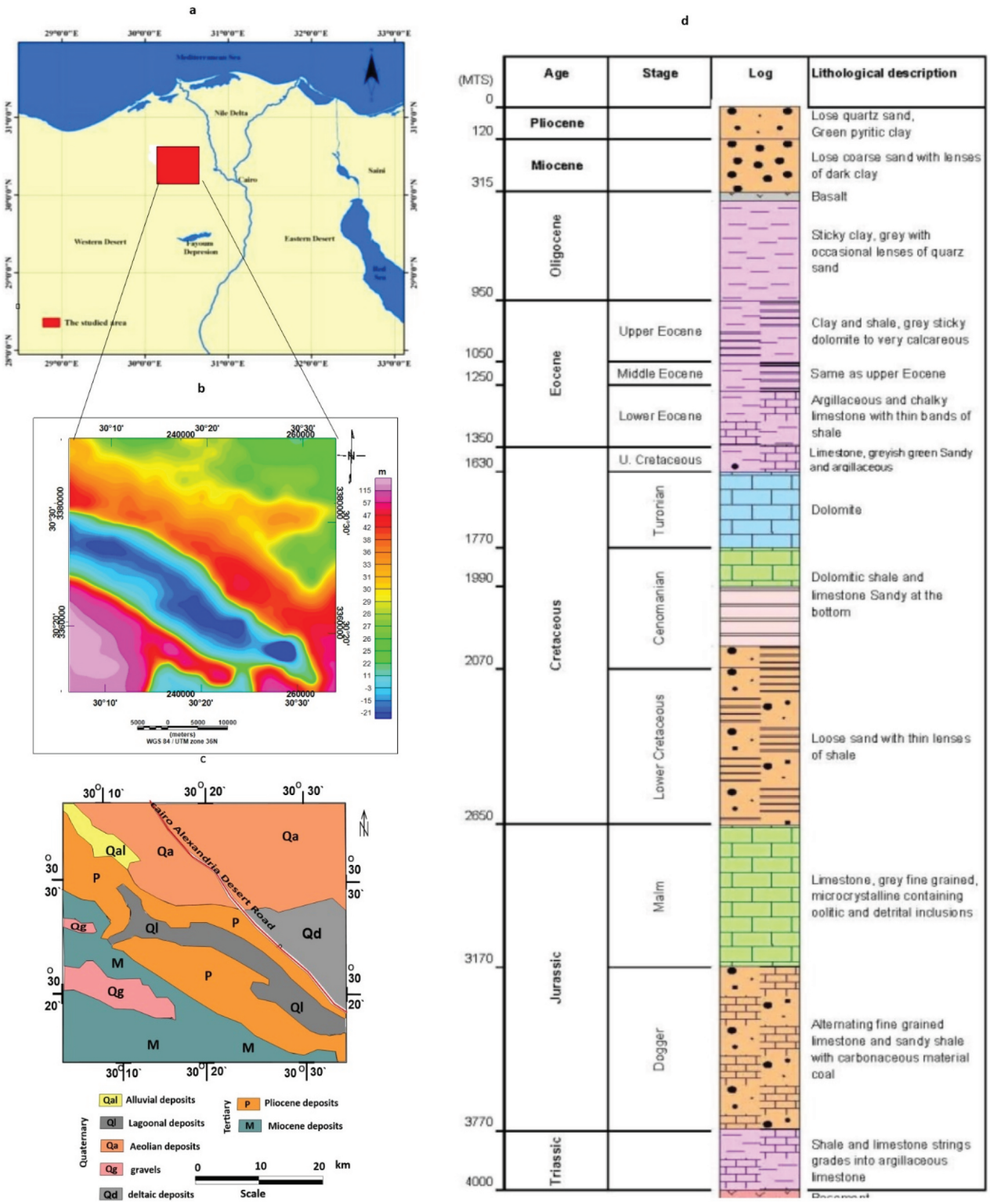


**Figure 1.** A: location map, b: topographic map, c: geologic map (modified after Conoco 1987), d stratigraphic section of Wadi El Natrun well (modified after Shata and El Fayoumi 1967).

occupy the south and southwest of the area under study. Quaternary sediments occupying the north of the study area are composed mainly of clastic deposits with clay intercalations. Sand dunes occupy the southern part of the investigated area.

The subsurface stratigraphy of Wadi El-Natrun area is described from a drilled well that reached the basement rocks (Figure 1(d)). The drilled well indicates that the Pliocene sediments are represented by loose quartz sand and green pyrite clay of thickness 120 m. The Miocene deposits at a depth ranging from 120 to 315 m consist of coarse sand with the lenses of dark clay. Oligocene rocks comprised basalt clay with lenses of quartz sand were viewed at depth from 315 to 950 m. Eocene rocks include different geologic units such as clay, shale, sticky dolomite, argillaceous and

chalky limestone were displayed at depth from 950 to 1350 m. Cretaceous deposits consist of limestone, dolomite, dolomitic shale, and loose sand at depths from 1350-to 2650 m. Jurassic sediments are limestone and sandy shale from 2650 to 3770 m, while Triassic deposits are shale and limestone at a depth of 3770–4000 m. Finally, the basement rocks were detected at a depth of 40,000 m.

## 3. Methodology

The authors used gravity data collected by the Egyptian General Petroleum Corporation (EGPC) (1976); the data was reduced for different corrections such as drift, tide, latitude, and elevation correction. The Bouguer anomaly (BA) map (Figure 2(a)). The BA map refers to high gravity values in the central and southern parts but the low gravity values occupying the northeastern and western portions. The gravity values range from −23.7 to – 5.4 mGal.

### 3.1. Gravity filtering

Different gravity filters are applied to the gravity data, such as low and high pass and upward and downward techniques. The power spectrum curve (Figure 2(b)) was used to determine the wavenumber and the average depth of the deep and shallow sources, where the depth of an 'ensemble' of sources is easily determined by measuring the slope of the energy (power) spectrum and dividing by 4 π.

$$h\ (depth) = -S/4\pi \text{ where } S \text{ is a slope}$$

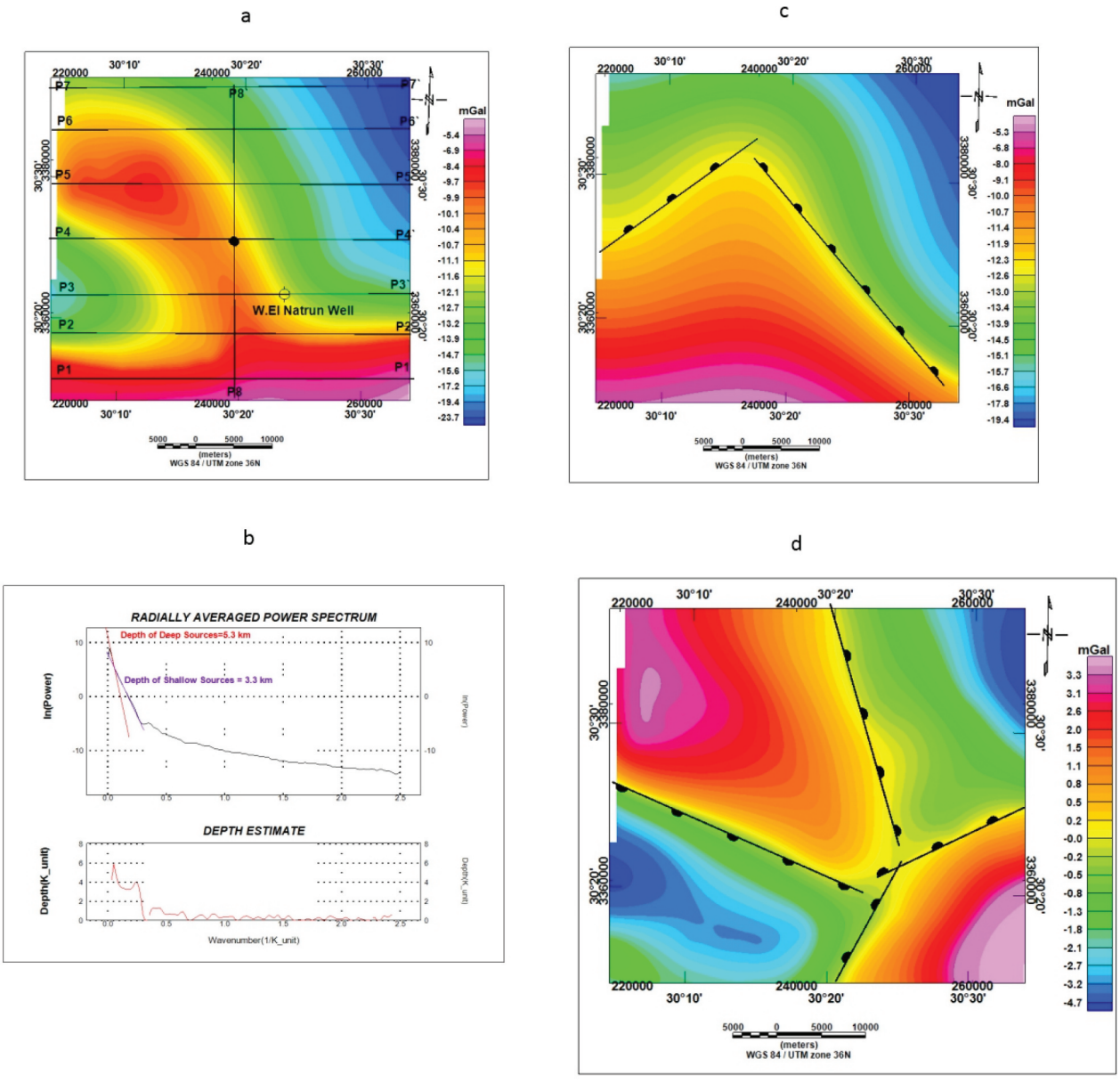


Figure 2. A: bouguer anomaly map with locations of 2-D profiles, b: power spectrum curve, C: low pass filter (regional) map showing two fault elements of NE-SW and NW-SE trends, d: high pass filter (residual) map showing different fault elements of NE-SW, NW-SE and N-S trends.

The deep sources are at a depth of 5.3 km, whereas the shallow sources are at a depth of 2.3 km. Moreover, the low and high pass filter are carried out at wavenumber 0.0562 1/k_unit.

#### 3.1.1. Low pass (regional) map

The low-pass filter smoothes the input data by the application of a convolution filter to the data. Features in the data that are shorter than the short wavelength cut-off will be removed. The convolution filter is designed using the method of Fraser, 1966. The low pass map represents a regional map (Figure 2(c)) which reflects regional features showing two regional fault elements dissecting the investigated area of NE-SW and NW-SE directions.

#### 3.1.2. High pass (residual) map

A high-pass filter sharpens the input data by the application of a convolution filter. Features in the data that are longer than the long-wavelength cut-off will be removed. The high pass (residual) map (Figure 2(d)) reflects different anomaly amplitudes of high and low gravity values where the northwestern and southeastern regions inhabited high gravity anomalies. Still, the southwestern and northeastern parts refer to common gravity anomalies. Also, the high pass map shows many structural features of trends as NE-SW, NW-SE, N-S and NNE-SSW.

#### 3.1.3. Upward continuation maps

The upward continuation technique is applied to smooth the gravity anomalies to separate the shallow sources from the deeper sources of the potential field at an elevation higher than the field is measured. Upward continuation is used to smooth out near-surface effects (Telford, 1990). The upward continuation technique was applied in the current study at distances 2000, 3000, 4000 and 5000 m (Figure 3). These maps reveal that the maps become smoother up to the depth of 5000 m. The shallow sources are suppressed, and deep sources are smoother at greater depth.

#### 3.1.4. Downward continuation maps

Downward continuation enhances sources at a specified depth. This procedure can be used as an interpretation tool to determine the depth of a causative body. The downward continuation in the current study is carried out at depths of 100, 500, 1000, and 2000 m, where the maps at depths 100 and 500 m are more or less similar to the original Bouguer anomaly map but at a depth of 1000 m, the anomalies started to distort and diminish at a depth of 2000 m (Figure 3)

### 3.2. Gravity derivatives

Gravity derivatives tend to sharpen the edges of the gravity anomalies and enhance shallow sources. Many techniques are concerned with detecting the edges of potential field anomalies (gravity) generated by geological structures. At present, edge detectors constitute an essential step in the potential field data interpretation (Blakely and Simpson 1986a; Narayan et al. 2016).

#### 3.2.1. First horizontal derivative (FHD)

The FHD technique is used extensively to delineate the boundaries of density contrasts from gravity data to detect the edges caused by fault elements or geological boundaries of rock units (Odek et al. 2013). The locations of structural features are indicated by the maximum FHD value, where the interpreted faults from FHD are represented by black lines (Figure 4(a,b)). The first horizontal derivative in both X and Y directions indicates that fault elements at the west and south of the study are NW-SE and N-S trends.

#### 3.2.2. First vertical derivative (FVD)

The first vertical derivative map is applied to give a sharper picture than the original map of the Bouguer. The FVD is used to delineate high-frequency features. The FVD map (Figure 4(c)) reveals faults at the west and centre of the investigated area, where the zero contours represent the edges of density bodies.

#### 3.2.3. Tilt angle derivative (TAD)

In potential field methods, the tilt angle technique is expressed as the ratio of the vertical derivative to the horizontal derivative of anomaly. In the tilt angle map, 0° contours define structure edges. The TAD defined by (Miller and Singh 1994; Verduzco et al. 2004) is as follows

$$TAD = \tan^{-1}\left[\frac{\partial g/\partial z}{\sqrt{(\partial g/\partial X)^2 + (\partial g/\partial y)^2}}\right] \quad (1)$$

Many authors have carried out the tilt angle analysis for delineating the locations of structural features (Williams et al. 2005; Blakely and Simpson 1986b; Hsu et al. 1996; Wijns et al. 2005; Miller and Singh 1994; Phillips et al. 2007; Ansari and Alamdar 2011; Oruc 2010; Cascone and Campbell 2012; Yuanyuan et al., 2010; ;Ghosh, 2016). The TAD is applied on the Bouguer map in the current study to delineate the structure features (Figure 4(d)) where the zero contours refer to edges of structures of different directions as NE-SW, NW-SE, E-W and N-S.

### 3.3. Quantitative gravity interpretation

The quantitative gravity interpretation is carried out to determine the depth of crystalline (basement) rocks through different techniques such as Euler deconvolution, 2-D gravity inversion and 3-D gravity inversion.

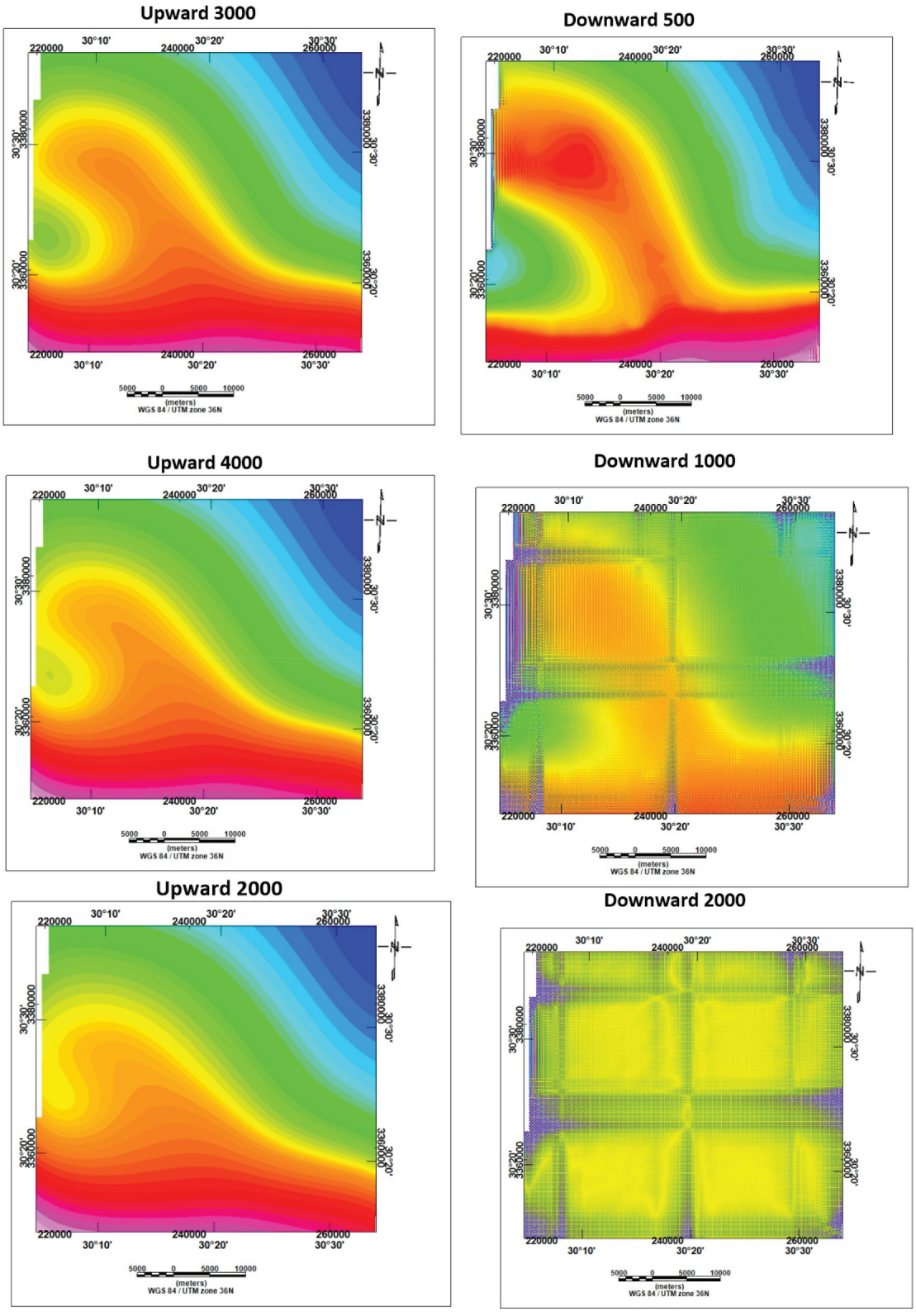


**Figure 3.** Upward and downward continuation.

### *3.3.1. Euler deconvolution*

The crystalline rocks' depth and structural features' locations are delineated through the Euler deconvolution technique. According to Thompson (1982), Euler's equation can be solved as the following

$$(x - x_0)\frac{dF}{dx} + (y - y_0)\frac{dF}{dy} + (z - z_0)\frac{dF}{dz} = -NF \quad (2)$$

where $x_o$, $y_o$, and $z_o$ represent the location's depth sources, F is the gravity field acquired at axes (x, y, z), and N is the Euler's structural index (SI). The depth for gravity source depends on the type of SI, which ranges from 0 to 2. We have used SI = 0 in the current study on the Bouguer map. The Euler deconvolution delineates the structure or contact at the different levels of a depth corresponding to the crystalline rocks. The solutions of

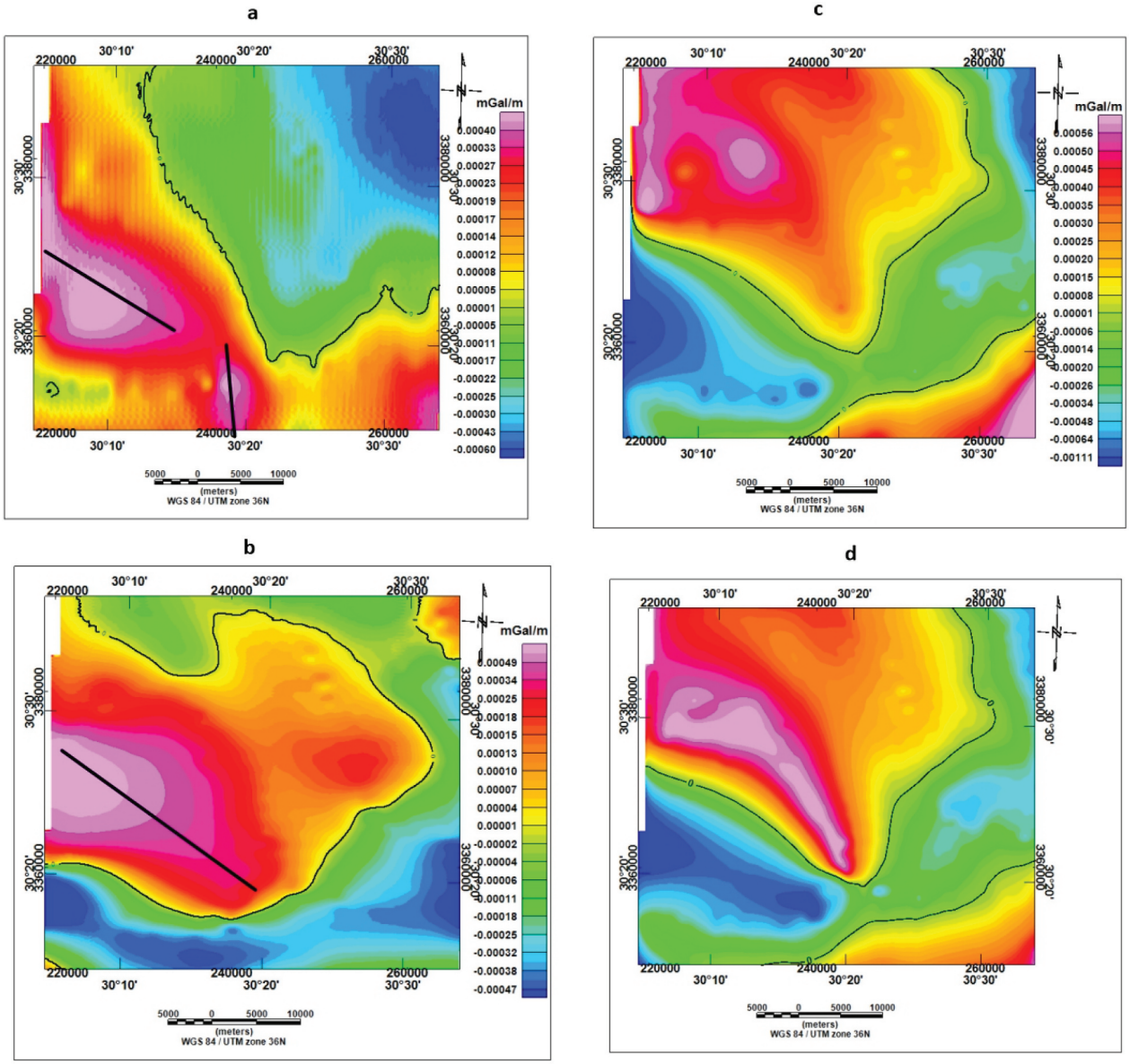


**Figure 4.,** A: first horizontal derivative on X-direction, b: first horizontal derivative on Y-Direction, c: first vertical derivative, d: tilt derivative.

Euler deconvolution of SI = 0 (Figure 5) show depths of gravity source ranging from 3000 m to more than 5000 m.

Figure 6 represents the integrated map for structural trends from different techniques where this map reflects compatibility between the different techniques for delineating the structural trends in the study area

### 3.3.2. 2-D gravity modelling

The 2-D gravity modellings are applied at eight profiles as in Figure 7 using GM-SYYS software (Montaj 2015), seven of them are of W-E direction of the length of 46 km for each profile the eighth one of S-N direction of the length of 41 km. The third profile passes through the borehole drilled to reach the upper surface of basement rocks at a depth of 4000 m. The basement depth, estimated through all profiles, ranges from 3200 m at the beginning of profile 8 to 5600 m at the end of profile 7.

### 3.3.3. 3-D gravity modelling

The 3-D gravity modelling technique is applied in the current study using Montaj 2015 to estimate the actual depth of basement rocks from 3-D gravity inversion. The initial model for 3-D gravity inversion was utilised from results of 2-D modelling using 2.3 g/cm$^3$ for sedimentary cover and 2.67 2.3 g/cm$^3$ for basement rocks. Figure 8 shows the outputs of 3-D gravity inversion using Oasis Montaj, 2007 n. Figure 7(a) represents an observed gravity map, b represents a calculated gravity map, c represents

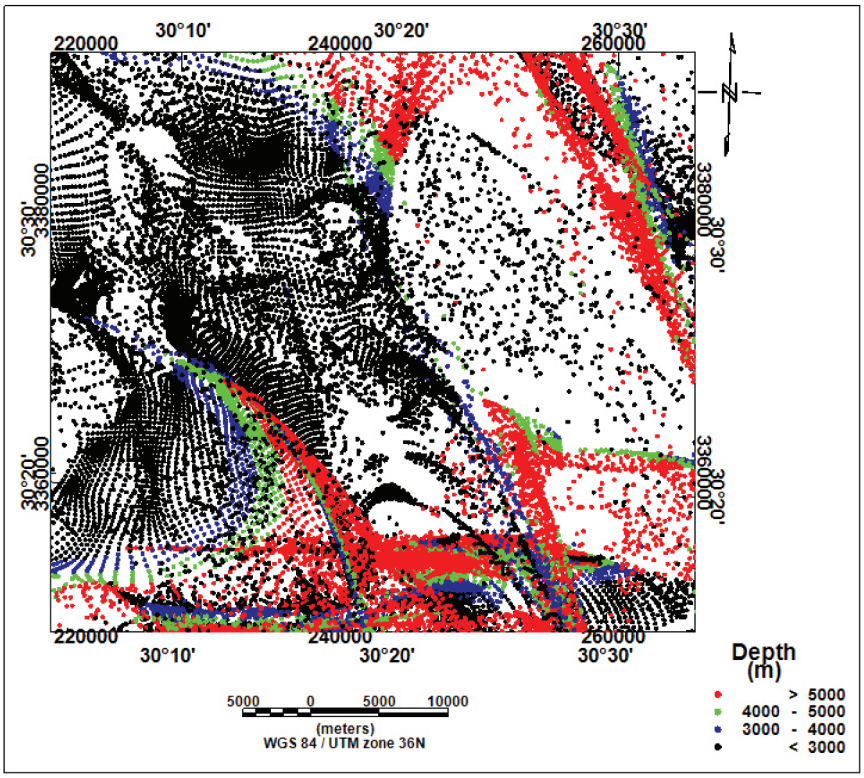


**Figure 5.** Euler solutions at structural index zero.

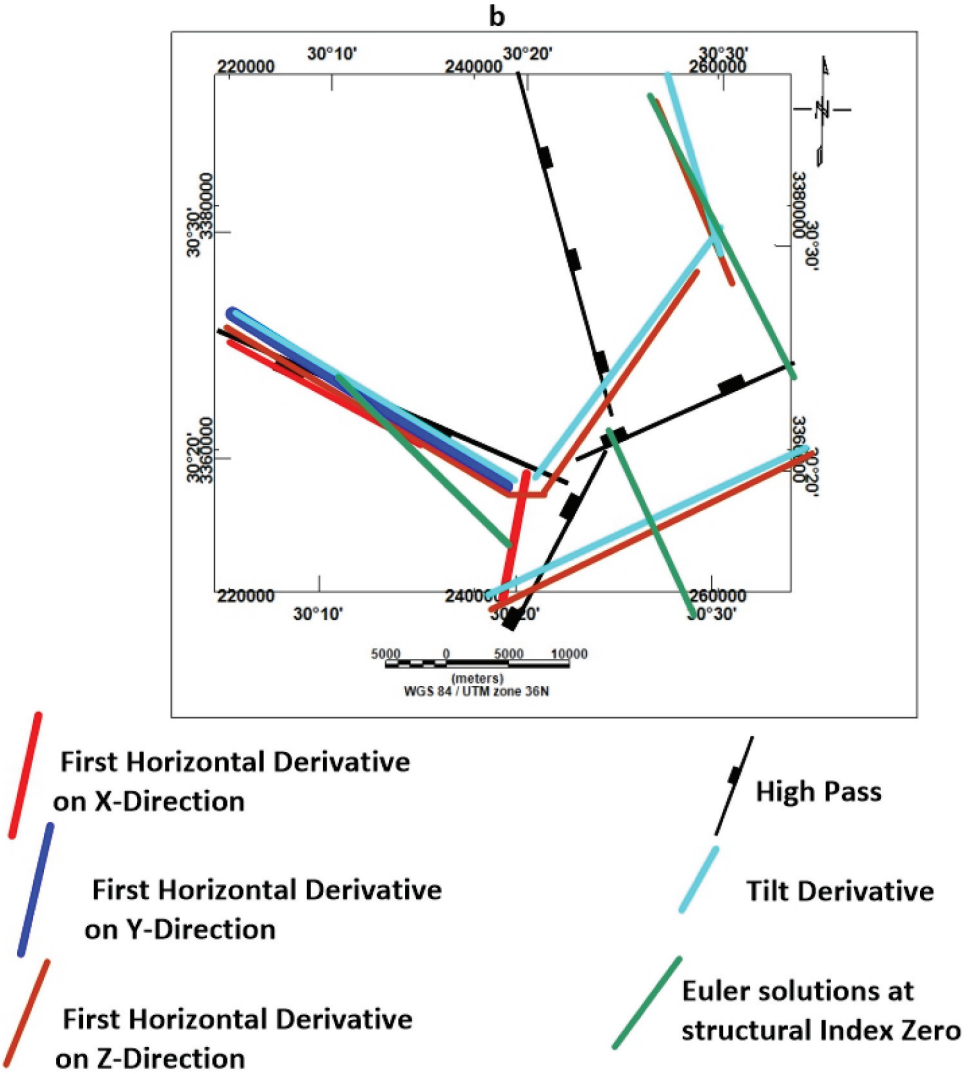


**Figure 6.** Structural trends from different techniques.

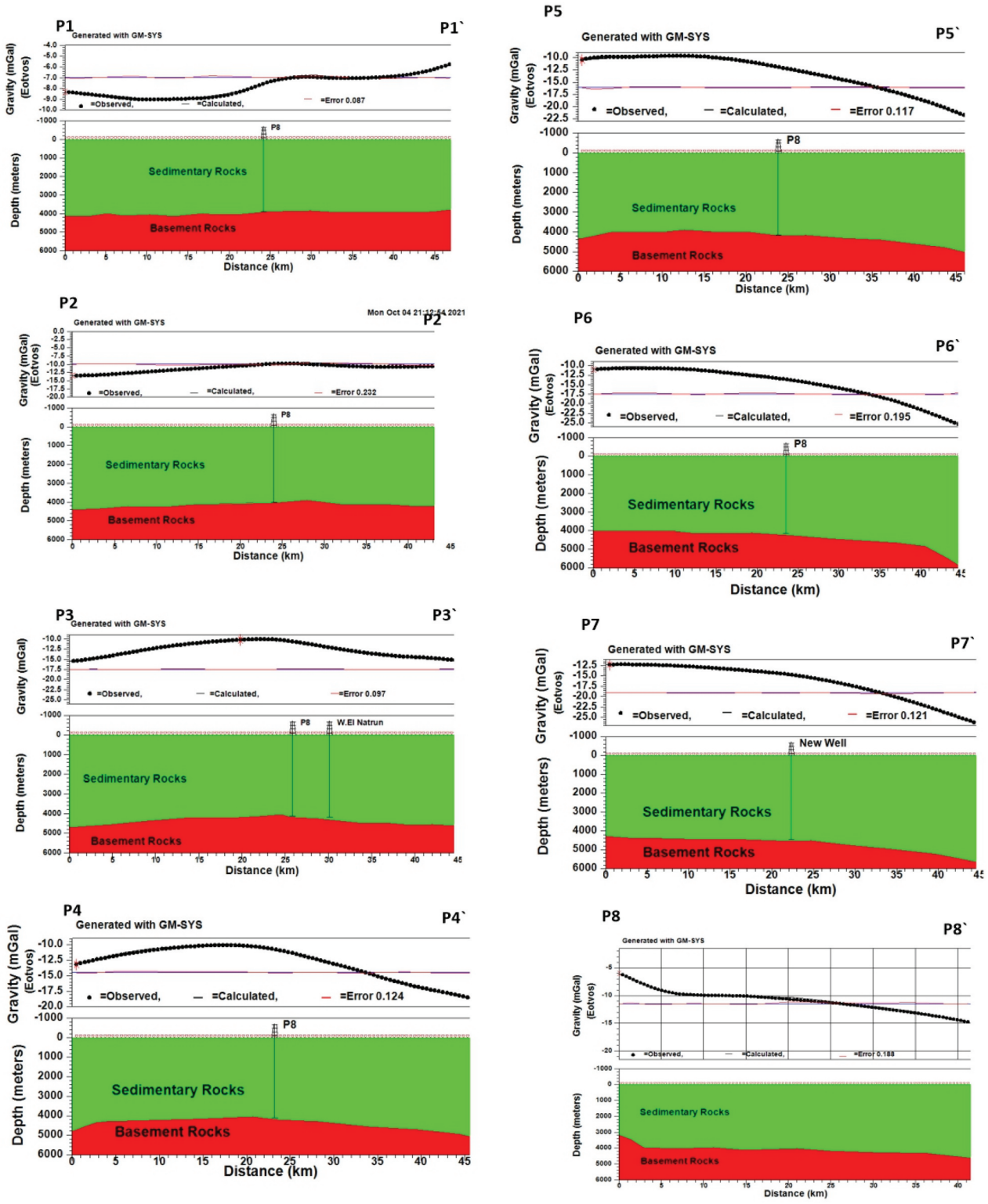


**Figure 7.** 2-D gravity modelling along with profiles 1–8, using Oasis Montaj, 2015, where the density of sedimentary cover is 2.3 g/cm$^{3,}$ and the density of basement rocks is 2.67 g/cm$^{3}$.

an error gravity map ranging from −1.6 to 1.1 mGal. The depth of basement relief ranges from 3800 m to 5300 m; this map shows two uplifts of depth to the basement about 3800 m and two basins of depth about 5300 m.

## 4. Discussion

The interpretation of gravity data is used to delineate the structural features that cross the area under study and control the distribution of groundwater and oil accumulation distribution in the study area.

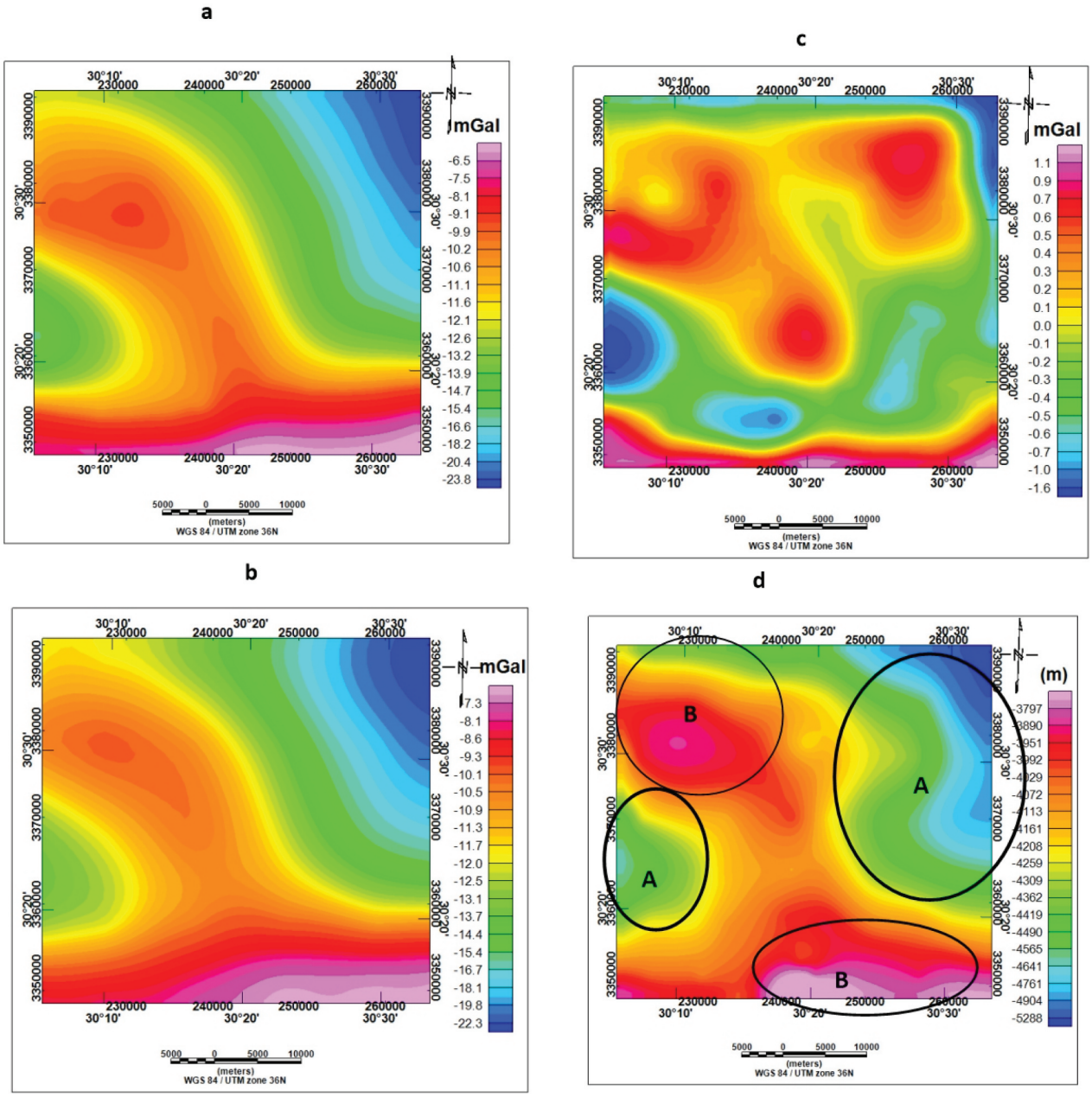


**Figure 8.** 3-D gravity inversion using oasis Montaj (2015) (GM-Sys-3D) a, observed gravity map, b: calculated gravity map, d: error gravity map, e: basement relief map from 3-D gravity inversion where zone A represents basins and zone B, represents uplifts.

Many companies that work in Egypt in the petroleum field extract the oil from the Western Desert. The study area is located in the northeastern part of the Western Desert, where the thickness of the sedimentary cover is available for oil accumulation. The area under study is affected by different fault elements in different trends as NE-SW, NW-SE, E-W and N-S. The upward continuation refers to the depth of deep sources reaching more than 5000 m. The derivatives such as the first horizontal, vertical and tilt angle derivative indicate that the locations and trends of fault elements are conformed together. The most structural features are concentrated in the western and southern parts of the study area. The results of 2-D gravity inversion and 3-D gravity inversions are compatible. The depth of basement rocks of the borehole drilled at the centre of the study area (Wadi El Natrun well) is 4000 m; the estimated depth of the basement at this site of the borehole is 4225 m. The difference between real depth from the borehole and estimated depth from gravity inversion is 225/4000, which equals 5.6% of the error ratio.

## 5. Conclusion

From the gravity interpretation results, we can conclude that most structural features are located in the western, central, and southern parts of the investigated area. The structural trends are NE-SW parallel to the Gulf of Aqaba, NW-SE parallel to the Gulf of Suez,

N-S parallel to the Nile Valley and E-W parallel to the Mediterranean Sea. The depth of basement rocks ranges from 3800 to 5300 m. The western and eastern parts represent basins that are suitable for oil accumulations.

## 6. Recommendation

The study area lies in Natrun basin, northeastern of Abu-Gharadig basin, east of Alamein basin, and north of El-Gendi basin, where these areas contain a lot of oil fields. For these reasons, the study area may be highly potential for oil accumulation. The authors recommended more detailed seismic reflection in the eastern and western parts of the study area.

## Disclosure statement

No potential conflict of interest was reported by the author(s).

## ORCID

Sultan Awad Sultan Araffa http://orcid.org/0000-0002-7098-918X

## References

Abdel Zaher M, Elbarbary S, Sultan SAA, El-Qady G, Ismail A, Takla EM. 2018. Crustal thermal structure of the Farafra oasis, Egypt, based on airborne Potential field data. Geothermics. 75:220–234. doi:10.1016/j.geothermics.2018.05.006.

Abu E-IMS. 1971. Landforms of Egypt. Cairo: American University Press; p. 281.

Ansari AH, Alamdar K. 2011. A new edge detection method based on the analytic signal of tilt angle ASTA for magnetic and gravity anomalies, Iran. J. Sci. Technol. 35(A2):81–88.

Araffa SAS, El-bohoty M, Abou Heleika M, Mekkawi M, Abd EL-Razek Enas M, Khalil A, Abd EL-Razek EM. 2018. Implementation of magnetic and gravity methods to delineate the subsurface structural features of the basement complex in central Sinai area. Egypt NRIAG Journal of Astronomy and Geophysics. 7(1):162–174. doi:10.1016/j.nrjag.2017.12.002.

Araffa SAS, Abdelazium M, Saleh SH, Dabour Ahmed A. 2021a. Hydrogeophysical Investigation at El Moghra Area, North Western Desert, Egypt. Environmental Earth Sciences. 80(2):55. doi:10.1007/s12665-020-09332-5.

Araffa SAS, Abdelazium M, Saleh SH, Dabour Ahmed A. 2021b. Gravity interpretation for delineating subsurface structures and depth of basement at El Moghra area, North Western Desert, Egypt. NRIAG Journal of Astronomy and Geophysics. 10(1):270–278. doi:10.1080/20909977.2021.1913364.

Blakely RJ, Simpson RW. 1986a. Approximating Edges of source bodies from magnetic or gravity anomalies. Geophysics. 51(7):1494–1498. doi:10.1190/1.1442197.

Blakely RJ, Simpson RW. 1986b. Approximating edges of source bodies from magnetic or gravity anomalies. Geophysics. 51(7):1494–1498. doi:10.1190/1.1442197.

Cascone L, Campbell S, 2012. ACLAS: a new automatic method of defining potential field lineaments using coherency analysis. In: Proc. SEG Annual Meeting, 2012 Nov 4-9, Las Vegas, USA, SEG- 2012–1254.

CONOCO. 1987. Geological map of Egypt. Egyptian general authority for petroleum (UNESCO joint map project), 20 sheets, Scale 1: 500,000. Egypt:Cairo.

Egyptian General Petroleum Corporation (EGPC) (1976): Bouguer anomaly map, Scale1:100000.

Elbarbary S, Araffa SAS, El-Shahat A, AbdelZaher M, Khedher KM. 2021. Delineation of water potentiality areas at Wadi El-Arish, Sinai, Egypt, using hydrological and geophysical techniques. Journal of African Earth Sciences. 174:104056. doi:10.1016/j.jafrearsci.2020.104056.

Ghosh GK. 2016. Interpretation of Gravity Data using 3D Euler Deconvolution, Tilt Angle, Horizontal Tilt Angle and Source Edge Approximation of the North-West Himalaya. Acta Geophysica. 64(4)Aug. 2016:1112–1138. 10.1515/acgeo-2016-0042.

Hsu SK, Sibuet JC, Sibuet CTS. 1996. High-resolution detection of geological boundaries from potential field anomalies. An Enhanced Analytic Signal Technique, Geophysics. 61(2):373–386. doi:10.1190/1.1443966.

Ibraheem Ismael M, Elawadi Eslam A, El-Qady Gad M. 2018. Structural interpretation of aeromagnetic data for the Wadi El Natrun area, northwestern desert. Egypt, Journal of African Earth Sciences. 139:14e25.

Miller HG, Singh V. 1994. Potential field tilt – a new concept for location of potential field sources. J Appl. Geophys. 32(2–3):213–217. doi:10.1016/0926-9851(94)90022-1.

Montaj O. 2015. Geosoft mapping and processing systems, Geosoft Inc., Suit500, Richmondst. West Toronto (ON Canada): N5UIV6.

Narayan S, Sahoo SD, Pal SK, Kumar U, Pathak VK, Majumdar TJ, Chouhan A. 2016. Delineation of structural features over a part of the Bay of Bengal using total and balanced horizontal derivative techniques. Geocarto Int. 32(1):1–16.

Odek A, Otieno AB, Ambusso WJ, Githiri JG. 2013. 2D-Euler deconvolution and forward modeling of gravity data of Homa-Hills geothermal prospect. Kenya: JAGST; p. 15.

Oruc B. 2010. Edge detection and depth estimation using a tilt angle map from gravity gradient data of the Kozakl-Central Anatolia Region, Turkey. Pure Appl. Geophys. 168(10):1769–1780. doi:10.1007/s00024-010-0211-0.

Phillips JD, Hansen RO, Blakely RJ. 2007. The use of curvature in potential-field interpretation, explor. Geophys. 38(2):111–119. doi:10.1071/EG07014.

Said R. 1962. The geology of Egypt. Amsterdam and New York: Elsevier; p. 377.

Shata AA, El Fayoumi IF. 1967. Geomorphological and morphopedological aspects of the region west of the Nile delta with special reference to Wadi El-Natrun area. Bull Inst Desert d'Egypte. 13(1):1–38.

Telford WM, Geldart LP, Sheriff RE, and Keys DA. 1990. Applied Geophysics. Cambridge: Cambridge University Press.

Thompson DT. 1982. EULDPH: a new technique for making computer-assisted depth estimates from magnetic data. Geophysics. 47(1):31–37. doi:10.1190/1.1441278.

Verduzco B, Fairhead JD, Green CM, MacKenzie C. 2004. New insights into magnetic derivatives for structural mapping. The Leading Edge. 23(2):116–119. doi:10.1190/1.1651454.

Wijns C, Perez C, Kowalczyk P. 2005. Theta map: edge detection in magnetic data. Geophysics. 70(4):L39–L43. doi:10.1190/1.1988184.

Williams SE, Wijns C, Wijns C. 2005. Theta Map: edge detection in magnetic data. Geophysics. 70(4):L39–L43. doi:10.1190/1.1988184.

Yuanyuan L, Yushan Y, Tianyou L. 2010. Derivative-based techniques for geological contact mapping from gravity data. J. Earth Sci. 21(3):358–364. doi:10.1007/s12583-010-0099-8.